HHS Public Access

Author manuscript

Rep U S. Author manuscript; available in PMC 2019 January 08.

Published in final edited form as:

Rep U S. 2009 October ; 2009: 4092–4097. doi:10.1109/IROS.2009.5354075.

Surgical Retraction of Non-Uniform Deformable Layers of Tissue: 2D Robot Grasping and Path Planning

Rik Jansen[*], **Kris Hauser**[†], **Nuttapong Chentanez**[†], **Frank van der Stappen**[*], and **Ken Goldberg**[†]

[*]Deparmtent of Information and Computing Sciences, Utrecht University, PO Box 80089, 3508 TB, Utrecht, The Netherlands [†]IEOR and EECS Departments, University of California, Berkeley, Berkeley, CA 94720-1777, USA

Abstract

Robotic surgical assistants (RSAs) have the potential to facilitate surgeries and reduce human fatigue. In this paper we focus on *surgical retraction*, the common surgical primitive of grasping and lifting a thin layer of tissue to expose an underlying area. Given a 2D cross-sectional model of heterogeneous tissue with embedded structures (such as veins) and a desired underlying exposure region, we present an algorithm that computes a set of stable and secure grasp-and-retract trajectories, and runs a 3D finite element (FEM) simulation to certify the quality of each trajectory. To choose secure candidate grasp locations, we introduce the *continuous spring method* and combine it with the Deformation Space (D-Space) approach to grasping deformable objects with a linearized potential energy model based on the locations of embedded bodies. Experiments show that this method produces many of the same grasps as an exhaustive computation with an FEM mesh, but is orders of magnitude cheaper: our method runs in $O(\upsilon \log \upsilon)$ time, when υ is the number of veins, while the FEM computation takes $O(pn^3)$ time, where n is the number of nodes in the FEM mesh and p is the number of nodes on its perimeter. Furthermore, we present a constant tissue curvature (CTC) retraction trajectory that distributes strain uniformly around the medial axis of the tissue, by moving the gripper such that the tissue follows a constant-curvature, constant-length arc. 3D FEM simulations show that the CTC achieves retractions with lower tissue strain than circular and linear trajectories. Overall, our algorithm computes and certifies a high-quality retraction in about one minute on a PC.

I. INTRODUCTION

Robotic surgical assistants (RSAs) such as The Intuitive Surgical's daVinci™ system are increasingly being adopted into the operating room because of their ability to enhance a surgeon's precision and dexterity in laparoscopic procedures [8], [21]. But they are currently teleoperated directly as slave devices completely under the surgeon's control. Computer assistance of commonplace surgical tasks could alleviate the workload of the surgeon, allowing him or her to focus attention on more critical components of the surgery. It may also facilitate laparoscopic surgery with three or more manipulators, which may enable surgeons to perform more complex procedures than currently possible. Furthermore, automation may enable RSAs to perform procedures in battlefields, where trained medical

personnel are in short supply, as well as in remote locations, where large time delays hamper direct teleoperation [22].

This paper describes initial steps toward automating *retraction* in robotic surgery. In many surgical procedures, it is necessary to reveal an area of interest that is covered by an outer layer (e.g. skin). In order to do so, incisions must be made in the covering tissue. This will result in a layer of tissue, attached to the remaining tissue at only one side. A gripper may then be used to lift and retract the free end of the tissue layer (Fig. 1). We assume the incisions have been given, and we consider the problem of retracting a thin layer of tissue using a 2 point-jaw. The grasp location, jaw separation distance, and motion of the gripper must be chosen to balance two competing objectives: providing the surgeon with a clear view and good accessibility on the underlying area of interest (the exposure objective), while avoiding tissue damage (the strain objective). We set a maximum permissible tissue strain as a tissue damage criterion. Before executing a retraction on the real patient, the objectives must be *certified* by simulating the retraction with a 3D finite element model (FEM) of the tissue.

Although the tissue retraction takes place in 3D space, we restrict the motion of the gripper to a 2D cross-section of the tissue, as illustrated in Fig. 2. The gripper then has a 4D configuration space, and our retraction problem seeks a path in configuration space that achieves the specified objectives. We consider homogeneous as well as heterogeneous tissue containing veins, which we illustrate by embedding a number of stiffer parts in the softer surrounding tissue. The main objective of retraction is moving the tissue above the line-of-sight AB.

Since RSAs should act responsively to the quickly changing environment, we seek to reduce the amount of time we run relatively expensive FEM simulations. To do so, we decompose the 2D cross-section of tissue into orthogonal 1D components. Tangential to the layer, the tissue is treated as a cantilever beam; perpendicular to the layer, the tissue is modeled by an infinite number of linear springs. In the perpendicular direction, the *continuous spring model* is used to quickly determine a set of candidate grasp locations that make use of tissue heterogeneity to ensure locally *stable* grasp. For homogeneous tissue, all locations are locally equivalent, so we sample uniformly along the tissue. We find locally *secure* grasps using a method similar to the D-Space algorithm proposed by Gopalakrishnan and Goldberg to compute deform closure grasps [7]. Along the tangential direction, we use a cantilever beam model to derive an analytical solution for the *constant tissue curvature* (CTC) retraction trajectory, given a grasp location.

Experiments show that the spring model is able to find many of the same stable and secure grasps that would be computed by the original D-Space algorithm, while improving running time by orders of magnitude. We also show the CTC trajectory causes lower tissue strains than circular and linear trajectories. Combining the candidate grasp locations for heterogeneous tissue with the CTC trajectory, we certify each candidate retraction using the FEM simulator, evaluate the exposure and strain objectives, and pick the best retraction for execution. The combined algorithm can typically produce and certify high-quality retraction trajectories in about one minute on a PC.

II. RELATED WORK

A. Robotic surgical assistants

Several robots have been proposed for minimally invasive laparoscopic surgery, for example by Cavusoglu et. al. [4], Guthart and Salisbury [8], and Madhani et. al. [14]. The Intuitive Surgical's daVinci ™ system has been used in thousands of surgical procedures [8]. The surgeon uses a console with visual and tactile feedback to teleoperate a pair of manipulator arms that enter the body cavity. A variety of methods address improving the precision of such robots, including steady-hand systems [21] and motion scaling [8]. Nevertheless, these procedures remain under direct control of the surgeon. Our work considers semi-supervised operation of such robots. There has been some precedent for the use of semi-supervised robots in specific medical applications, such as neurosurgery [20], radiation therapy [23], and prostate brachytherapy [6].

B. Grasping deformable objects

A large body of work has addressed grasping and fixturing of rigid objects (see Bicchi and Kumar [2] for a survey), and a number of researchers have looked into this work to deformable objects. Cheong, et. al addressed fixturing problems for an articulated chain of polygons [5]. Cai, et. al. and Menassa et. al. investigated deformable sheet-metal parts while minimizing part deformation [3], [16]. Howard and Bekey used a learning approach to enable grasping of deformable objects using tactile feedback [11]. Yu et. al. studied the behavior of controllers for grasping soft tissue [25].

The notion of D-Space was introduced by Gopalakrishnan and Goldberg [7], to characterize stability and release resistance of deformable parts modeled by a FEM mesh. A configuration in D-Space is represented by all DOFs of the nodes of the mesh. The free space in D-Space consist of topology preserving, collision free configurations. Stable configurations require positive work to release the object from its grasp. An algorithm for finding an optimal jaw separation distance was also introduced for a two-point gripper that balances the energy needed to release the part against the energy needed to compress it into plastic deformation [7]. We use a simplified version of this technique to select secure grasps of a thin tissue layer.

C. Manipulating deformable objects

A number of researchers have addressed motion planning for deformable linear objects such as ropes and cables. Latombe et. al. describe a sampling-based motion planner for rope manipulation with two cooperating robot arms [19]. Kavraki et. al. describe a method for computing energy-minimizing curves subject to manipulation constraints, and apply them to surgical suturing problems [17]. Holleman et. al. and Lamiraux and Kavraki developed path planners for elastic surface patches [10], [13]. The surface patch is modeled as a Bezier surface with low bending energy, and a sampling-based planner is used to plan the path.

Other work has addressed planning for volumetric deformations. Rodriguez et. al. applied sample-based planning to deformable objects in deformable 3D environments [18]. Alterovitz et. al. used a numerical optimization approach to plan needle paths in 2D

deformable tissue for prostate brachytherapy [1]. Hirai et. al. used visual feedback to control points in 2D deformable tissue [9]. This approach has been considered for applications in breast biopsies [15] and prostate brachytherapy [24].

III. PROBLEM STATEMENT

A. Tissue and Robot Modeling

We model the tissue as a 3D elastic deformable body E. For simplicity we assume that E is a thin layer of uniform thickness having known material properties (and may be heterogeneous). For simulation purposes, E is represented into a tetrahedral FEM mesh. Heterogeneous tissue is modeled by a mesh with varying stiffness.

The robot gripper is modeled by two point contacts. We restrict the motion of the gripper to a planar cross section of 3D space. In the rest of this paper, we will take a frame of reference such that the cross section is spanned by the x-y plane, and gravity acts in the $-y$ direction. The tissue's bottom edge coincides with the horizontal axis, and is fixed at the right side.

We denote the space of all possible configurations of the robot on the plane as C. Throughout the discussion, we will describe a configuration $c \in C$ of the robot as a vector (x_1, y_1, x_2, y_2). Section IV-D will make use of a different $(x_1, y_1, \theta, \sigma)$ representation, where θ is the angle between the two jaws (as measured relative to the x-axis) and σ is the distance between the two jaws.

We denote the D-Space of all 3D FEM mesh configurations as D. A configuration $q \in D$ describes all positions of the simulation nodes. We forward simulate FEM dynamics using the method of Irving et. al. [12]. Our retraction selection algorithms make the assumption that the tissue is damped and velocities of the jaws remain low, such that the tissue moves smoothly between time steps and its motion can be approximated as a quasi-static process.

B. Retraction Trajectories

We describe a retraction with a robot trajectory $c(t) : [0, T] \mapsto$ C, for some termination time T. We assume that at time $t = 0$, the jaws are instantaneously placed at points on the perimeter of the tissue. In other words, we do not consider how the robot moves before it makes initial contact. After we contract the jaws a certain distance, the motion of the tissue in response to $c(t)$ can be computed by evaluating the FEM simulation. Let this path be denoted $q_c(t) : [0, T] \mapsto$ D. During the trajectory, we keep the distance between the jaws fixed.

C. Visibility, Grasp Security, and Strain Objectives

Our problem is to produce a retraction $c(t)$ and a termination time T that meets the following objectives:

1. *Visibility.* Given the location B on the area of interest that lies farthest away from the camera, and the camera position A, we require that at time T, all the tissue at configuration $q_c(T)$ lies above line AB. This condition is illustrated in Fig. 2.

2. *Grasp security.* We require that the grasp points stay fixed relative to the tissue throughout the retraction (i.e., do not break contact or slip). We assume the friction coefficient μ between the gripper and tissue is known.

3. *Admissible strain.* The "maximum strain" measure we use in this paper is actually not the actual maximum strain, but rather a variant that is less prone to noise and discretization artifacts in the FEM mesh. Let $\epsilon_{1\%}(q)$ be the average strain of the 1% of volume elements with the highest strain in tissue configuration q. Let the "maximum strain" $\epsilon_{max}(c)$ be the maximum of $\epsilon_{1\%}(q)$ for all tissue configurations along the retraction. We require that $\epsilon_{max}(c)$ does not exceed a strain limit ϵ_L.

We assume that if the robot computes a certificate that a retraction $c(t)$ satisfies these objectives in the FEM simulation, then $c(t)$ is safe to execute. We also consider $\epsilon_{max}(c)$ as a soft objective function, such that given a number of retractions to certify, and a sufficient amount of computation time, we will pick the retraction that minimizes the maximum strain.

IV. METHOD

A. Overview of Generate-and-Test Approach

We seek efficient solutions to the retraction problem. Due to the high computational expense of FEM simulation, general-purpose methods (e.g., numerical optimization or sample-based motion planning) are prohibitively expensive. Instead, our approach generates a number of candidate retractions (up to a user-defined maximum), and tests the objectives of Section III-C by evaluating the FEM simulation.

To generate the retractions, we first pick a set of contact pairs p_a and p_b which are likely to be locally stable, using a simplified linear spring model. Each contact pair p_a and p_b defines a single candidate retraction, as follows. We first close the jaws to a distance that trades off stability against tissue strain. Then, holding the separation distance constant, we move the gripper along a trajectory that is optimal if the tissue layer is viewed as a homogeneous cantilever beam under no gravity. The following sections will describe how we generate each component of the retractions in more detail.

B. Choosing stable grasp locations

The first task in retraction is determining where to grasp the tissue. The locations we choose are locally optimal with respect to the grasp security and admissible strain objectives, while we consider the visibility constrain at a later stage. Gopalakrishnan and Goldberg [7] introduced the notion of D-Space for deformable tissue modeled by a FEM mesh. Grasps that are located at local minima in the elastic potential are considered *stable*, and they describe an algorithm that finds an optimal jaw distance between 2 jaws at perimeter nodes, by trading off stability against plastic deformation. Finding the optimal distance for a n-nodes mesh with p perimeter nodes takes $O(n^3p^2 + p^6 \log p)$ time.

We use the same concepts in our approach, but can find stable grasp positions considerably faster because our object is known to be a flat rectangular mesh. We further simplify the problem by requiring that the jaws must be directly opposite the mesh surface, as illustrated

in Fig. 3. Otherwise, the jaws would apply asymmetric forces to the tissue after compression, and would compromise our grasp security constraint. Thus, our problem is reduced to finding a horizontal translation x along the length of the tissue.

1) Stable grasps and escape energy: To find stable grasps, we examine the tissue under compression as a function of x. We let $k_{eq}(x)$ denote the *equivalent spring constant*, which represents the amount of force at x needed to compress the tissue a unit distance.

We characterize the stability of a grasp location x by its ability to resist shifting to a neighboring spring. That is, a grasp at x is *stable* if positive work is needed to shift the grasp from x to x'. This is precisely the case where x corresponds to a local minimum of $k_{eq}(x)$. Escaping the basin of attraction of a stable grasp requires sliding the grasp past a local maximum of $k_{eq}(x)$. We use the following *escape potential* metric to characterize the stability of a stable grasp location x:

$$Escape(x) = \min\left(k_{eq}(x_r), k_{eq}(x_l)\right) - k_{eq}(x)$$

where x_r and x_l are respectively the local maxima to the right and left of x.

Thus, to find all stable grasp locations and calculate their escape potential, we must simply find the extreme points of k_{eq}. Though, in principle, it would be possible to compute k_{eq} using the FEM model, we use a much faster *continuous spring model* approximation.

2) Locally stable grasp locations using a continuous spring model: In this section we will use a model for the tissue that approximates the tissue's compression behavior as a vertical linear spring along a slice through the tissue (Fig. 3). This approximation decouples each slice from its neighboring tissue, and therefore ignores interactions due to shear stress. If the tissue is sufficiently thin, shear stresses will not affect the compression behavior much.

Consider the line segment $s_{cross}(x)$ running vertically through the tissue between the jaws placed at x. We can decompose it into multiple line segments s_i with length $l_i(x)$, each of which has constant Young's moduli E_i. We'll consider the s_i as infinitesimal small bars and according to Hooke's law, any force F applied to such a bar having cross sectional area A_i and length $l_i(x)$ induces a displacement ΔL:

$$F = \frac{E_i A_i}{l_i(x)} \Delta L = k_i(x) \Delta L \quad (1)$$

After eliminating the cross sectional area, which is constant over all bars, we see that we can consider s_i as a spring with spring constant $k_i(x) = \frac{E_i}{l_i(x)}$. Stringing all these segments together, we treat $s_{cross}(x)$ as a serial spring with equivalent spring constant $k_{eq}(x)$:

$$k_{eq}(x) = \frac{1}{\sum_{i=1}^{n} \frac{1}{k_i(x)}} = \frac{1}{\sum_{i=1}^{n} \frac{l_i(x)}{E_i}} \quad (2)$$

where $l_i(x)$ describes the intersection length of veins i with $s_{cross}(x)$. In practice, for a thin slab of tissue, only a small number of veins are being intersected at any distance x along the tissue.

Since the veins are represented as polygons, we can compute the extreme points of k_{eq} using a sweep line algorithm. We note that the extreme points of $k_{eq}(x)$ are also extreme points of $\frac{1}{k_{eq}(x)}$, and $\frac{1}{k_{eq}(x)}$ is a sum of linear functions. Considering vertices of polygons as event points, we find when $1/k_{eq}(x)$ changes slope for each vertex encountered in the event queue. If the veins are represented by v vertices, sorting the queue takes $O(v \log v)$ time, and each of the v event points can be evaluated in $O(1)$ time, which leads to an $O(v \log v)$ running time overall.

Fig. 4 shows an example of the model and the equivalent spring constant function constructed by the sweep-line method using a fine polygonalization of the veins.

C. Choosing an optimal jaw distance

Once we have chosen a location to grasp the tissue, we must choose a compression distance σ. We use a criterion similar to that used in Gopalakrishnan and Goldberg [7] which balances the competing objectives of a secure grasp and low strain, in particular, we choose σ such that the energy needed to release the grasp is equal to the energy needed to exceed the strain limit. An important consequence of this criterion is that jaw compression can be reduced when the tissue is heterogeneous and the grasp location is locally secure (i.e., bordered by relatively stiff veins). In turn, this reduces the strain imposed on the tissue.

We choose σ as follows. Let the tissue at the grasp point have the equivalent spring constant k_{eq}. Compressing the jaws to distance σ will achieve strain:

$$\epsilon = \frac{L - \sigma}{L}$$

where L is the rest height of the tissue. The elastic strain limit ϵ_L imposes the constraint $\dot{\sigma} \geq (1 - \epsilon_L)L$. Given σ, the amount of energy needed to compress the spring to the strain limit is

$$U_L(\sigma) = \frac{1}{2} k_{eq} \left(\sigma - \left(1 - \epsilon_L\right)L\right)^2 \quad (3)$$

We also find the two locally stiffest parts of the tissue that neighbor the grasp positions. Pick the least stiff of the two, and let k_n denote its equivalent spring constant. If the tissue is

locally homogeneous, we set $k_n = k_{eq}$. The amount of energy U_n to compress the neighboring spring a distance σ equals:

$$U_n(\sigma) = \frac{1}{2}k_n\sigma^2 \quad (4)$$

We choose σ such that (3) and (4) are equalized. This value is given by:

$$\sigma = \frac{\sqrt{k_{eq}}(1-\epsilon_L)L}{\sqrt{k_{eq}}+\sqrt{k_n}} \quad (5)$$

We use $U_n(\sigma)$ (= $U_L(\sigma)$) as a grasp stability metric. Note that $U_n(\sigma)$ at grasp location x is proportional to $E_{scape}(x)$. Fig. 4 illustrates the ranking of several grasp points based on this metric.

D. Choosing a Retraction Trajectory

After finding grasp locations p_a, p_b and a jaw separation distance σ, we must find a path of the manipulator to retract the tissue. Some simple paths (e.g., straight lines and circular arcs) can achieve the retraction objectives without causing excessively high strains, because the largest strains are usually caused by the squeezing of the gripper. But, they do stretch the tissue unnecessarily. Therefore, we introduce a *constant tissue curvature* (CTC) trajectory that keeps the medial axis of the tissue stretch-free and bend with a constant curvature.

To compute this trajectory, we treat the tissue as a homogeneous cantilever beam that can bend and stretch, and ignore the effects of gravity. Since tissue is thin, the strain caused by stretching is much higher than the strain caused by bending. **** Our gripper will clamp the tissue on the free end and as the tissue remains attached to remaining tissue, we treat the fixed end as clamped as well. Given such boundary conditions, the tissue will obtain a configuration that minizes potential energy, which is comprised of bend energy and stretch energy. Since the tissue is thin, the stetch energy will be much larger than the bend energy. This entails that strains caused by stretching is much higher than strains caused by bending. Furthermore, our tissue needs to lie above the line of sight. Since our fixed end of the tissue lies in the same half-space, any curve that fullfills this contraint and is stretched, can be unstretched and still fullfill the constraint. As a result, stretching is unnecessary. *** Thus, we aim to keep the length of the tissue constant. With the length held constant, we also seek to minimize the maximum bending strain. In order to achieve a uniformly distributed strain, theories on beams prescribe that curvature should be constant, so the beam should form a circular arc. We are therefore interested in finding the retraction $c(t)$ that bends the tissue in a circular arc while keeping its length fixed.

We place a coordinate frame with its origin at the lower-right corner of the tissue. Let L denote the position of the grasp point. Along $c(t)$, the−lower edge of the tissue must describe a circular arc with constant length L but time-varying radius $R(t)$ and center $(0, R(t))$, as illustrated in Figure 5. At $t = 0$, we have $R(t) = \infty$and as t increases, $R(t)$ decreases, moving

the center of the circle along the y-axis toward the x-axis. At the end time $t = T$, the arc must lie to the right of the line-of-sight.

We compute the goal radius $R_g = R(T)$ to be tangent to the line-of-sight. With a bit of algebra, this can be shown to be:

$$R_g = \frac{|A - B||b_x a_y - a_x b_y| - (a_x - b_x)(a_x b_y - b_x a_y)}{(a_y - b_y)^2} \quad (6)$$

where $A = (a_x, a_y)$ and $B = (b_x, b_y)$. We linearly interpolate curvature to determine tissue radii $R(t)$ in intermediate time steps:

$$R(t) = R_g \frac{T}{t}$$

At the tissue configuration at time t, the medial axis of the tissue will coincide with an arc of the circle with center $(0, R(t))$, but with radius $R(t) - \frac{1}{2}h$. Sliding along this arc with arclength L, we compute the point $p(t)$:

$$p(t) = \left(\left(R(t) - \frac{1}{2}h\right)\cos\theta, \left(R(t) - \frac{1}{2}h\right)\sin\theta + R(t)\right)$$

$$\theta(t) = \frac{L}{R(t) - \frac{1}{2}h} + \frac{3}{2}\pi$$

where the angle θ is chosen to keep the arclength fixed. At $c(t)$, the projections of the jaw locations on the medial axis should coincide with $p(t)$. Incorporating the jaw separations σ, we present the equations of the final trajectory:

$$p_{pa}(t) = \left(R_a(t)\cos\theta(t), R_a(t)\sin\theta(t) + R_a(t)\right)$$

$$p_{pb}(t) = \left(R_b(t)\cos\theta(t), R_b(t)\sin\theta(t) + R_a(t)\right)$$

$$R_a(t) = R_g \frac{T}{t} - \sigma$$

$$R_b(t) = R_g \frac{T}{t} + \sigma - h$$

$$\theta(t) = \frac{L}{R_g \frac{T}{t} - \frac{1}{2}h} + \frac{3}{2}\pi$$

where p_{pa} and p_{pb} denote the location of the lower and upper jaw respectively. An illustration of such a path is given in Fig. 6

This previous analysis did not account for gravity or inhomogeneity. In either case, the tissue would no longer form a circular arc, and the tissue may droop below the line-of-sight. An

ad-hoc solution might simply set R_g lower than (6). We take a more principled approach where we generate an overly long retraction trajectory, and let the FEM simulation run only until all objectives are met, or some constraint is violated. *** As time increases, the radius of R(t) will increasingly become smaller than R_g. Bending strains in the tissue (which try to rectify the tissue to a straight configuration) will play a more dominant part as we increase and will eventually be able to compensate for gravity. ***

V. EXPERIMENTS

All results in this section were obtained on a tissue model having dimension of 5.0 cm in length and 0.44 cm in height and depth, and density of 1 g/cm^3. For 3D simulation, Young Modulus and Poisson Ratio of 40 kPa and 0.45 respectively for the tissue and 200 kPa and 0.45 respectively for the vein. We set ϵ_L = 0.5, and μ = 0.5 throughout all experiments. The gravity for the dynamic simulation is set to 9.8 m/s^2 downward.

A. Assessment of Grasp Selection Quality

We compare our continuous spring method of finding locally stable grasp locations to brute-force simulations with the commercial FEM package ANSYS. The FEM mesh contains 10,000 nodes and 160 pairs of opposite perimeter nodes. In ANSYS, we enumerated each pair of opposite perimeter nodes, contracted a unit distance and solved for the maximum strain in the tissue. The ANSYS simulation took 16 minutes and 32 seconds on a 1.8 GHz processor and 2 GB of RAM, while the spring method took 0.1 seconds. Fig. 7 shows the equivalent spring constant function k_{eq}, and indicates the top 15 grasp locations as computed by brute-force simulation and by our spring model. The spring model finds 8 out of 15 stable and secure grasp locations as computed by ANSYS.

B. Assessment of Retraction Path Quality

In the following experiments, we use our in-house 3D FEM simulator to compare the quality of our retraction trajectories (as described in Sec. IV-D) against linear and circular paths, which are attractive for their relative simplicity. We simulate the retraction by first compressing the jaws towards each other for an optimal distance (as described in Sec. IV-C) and then moving the jaws along the desired trajectory until the tissue is above the line-of-sight. We monitor the maximum strain during the simulation. For each grasp location, we run linear paths with (1) 60°and (2) 75° slopes, (3) a circular path and (4) the CTC trajectory. In the linear and circular paths, we adjust the jaw orientations such that they are perpendicular to the line from the fixed end to the jaws midpoint.

1) Experiments on homogeneous tissue: Fig. 8 plots the strain during the simulation on homogeneous tissue with gravity for two lines-of-sight for 10 uniformly sampled grasping locations. We can see that the CTC path performs better than the circular and linear paths in all cases, even for suboptimal grasp locations.

Repeating the same experiment for other lines-of-sight, we found that the CTC trajectory almost always outperforms the other paths, except when the line-of-sight lies close to the

fixed end of the tissue (approximately 25% away from the fixed end). In these cases, circular trajectories perform slightly better for certain grasp locations near the free end of the tissue.

2) Experiments on heterogeneous tissue: In this section, we consider a heterogeneous tissue containing 10 veins (Fig. 10). For all candidate grasp locations found the continuous spring method, we ran the 3D simulation using the linear, circular and CTC paths. Results are shown in Fig. 11. Both the CTC and the circular path are able to find the optimal jaw location between veins 3 and 4.

For suboptimal jaw locations, the CTC path usually outperforms other paths, except the circular path performs substantially better at jaw location 5. (Even under further scrutiny, we are unable to discern a clear cause for this behavior.) Apart from these occasional anomalies, this and other experiments suggests that the CTC trajectory still works well with heterogeneous tissue, even a homogeneity assumption was used in its derivation.

C. Optimal Grasp Locations for Varying Line-of-Sight

We also performed experiments to explore how the optimal grasp location computed by our algorithm varies depending on the lines-of-sight. We used homogeneous tissue, and exhaustively simulated the retractions computed for 50 grasp points uniformly distributed along the tissue. Fig. 12 shows that the optimal grasp locations vary, between 15% and 45% from the open end of the tissue. As the line-of-sight gets steeper or nearer to the fixed end of the tissue, the optimal grasp location moves closer to the free end of the tissue. We also found that the optimal jaw locations are insensitive to the friction limit, and in fact, no friction is required in the optimal retractions.

D. Efficient Simultaneous Certification and Selection Using Pruning

To choose the best of all candidate grasp locations computed by our spring model, we run the 3D FEM simulation for each candidate grasp location and choose the one that minimizes the maximum strain. Rather than run the simulation in full for each grasp location, we make use of two simple optimizations that improve the running time. Since we seek the retraction that minimizes the maximum strain $\epsilon_{max}(c)$, we can prune a retraction simulation early if the tissue strain exceeds the maximum strain computed for a prior retraction. We also terminate a simulation as soon as either the friction coefficient needed to hold the grasp exceeds μ or when the strain induced by the motion exceeds the plastic strain limit ϵ_L, which indicate failure.

Our experiments in the heterogeneous tissue of Fig. 10 suggest that this pruning technique reduces running time from 286s to 76s for 10 veins. On a more complex mesh with 20 veins, pruning reduces running time from 819s to 95s. In most cases, the simulation trials were pruned early on, as strain is accumulated quickly during the compression phase and at the beginning of retraction.

E. Optimal Retraction for a Wide Piece of Tissue

Fig. 9 shows a screenshot from a retraction computed by our algorithm on a 3.5 cm wide heterogeneous tissue. The full animation of this retraction accompanies this paper as a supplemental video.

VI. CONCLUSION AND FUTURE WORK

This paper introduced a method to compute a trajectory for a two-point gripper, moving in a plane, to retract a thin layer of tissue under visibility and tissue strain constraints. We propose a set of locally stable candidate grasps, where stability is characterized by the D-Space approach. Using a continuous spring approximation, we present an algorithm for finding candidate grasps that runs in $O(v \log v)$ time, when v is the number of veins embedded in the tissue. For each candidate grasp location, we compute a retraction trajectory that causes a cantilever beam model of the tissue to follow a constant curvature arc. These retractions are then certified using a 3D finite element simulator. Experiments suggest that 1) the continuous spring approximation computes many of the same grasp locations as a far more expensive FEM-based computation, and 2) constant-tissue-curvature paths produce lower tissue strains than circular or linear paths. Because our algorithm computes only a small number of candidate retractions, we can certify and select a high-quality retraction in about one minute on a PC.

In future work we hope to address more realistic manipulator models, with geometric and kinematic constraints that limit the accessibility of grasp points, as well as obstacles that limit the tissue's range of motion. With these constraints, regrasping may be necessary. Currently we use a strain metric as a proxy for tissue damage. *** Although our model is tested under circumstances involving gravity, our model does not take it into account. In terms of minimal energy configurations, gravity would add height energy, and minimization of the combination of bend energy and height energy should be investigated. *** A more sophisticated model would describes damage at the cellular level as a function of strain and duration of applied load. Our method also does not address retractions where the incision cuts along a line, and the manipulator must spread the incision to obtain a desired line-of-sight. Such retractions require a more three-dimensional reasoning than the method presented here. Simultaneous optimization of incision patterns and retraction trajectories is another line of work that would involve interesting tradeoffs: smaller incisions cause less trauma, but at the expense of larger tissue strains during retraction.

Supplementary Material

Refer to Web version on PubMed Central for supplementary material.

ACKNOWLEDGMENTS

This work was partially supported under National Institute of Health Research Award R01EB-006435–01A1. We thank M. Cenk Cavusoglu, Wyatt Newman, and Pieter Abbeel for inspiring discussions. We would also like to thank Ron Alterovitz and Vincent Duindam for their thoughts and advice. We thank Siamak Faridani for his help on ANSYS.

REFERENCES

[1]. Alterovitz R, Goldberg K, Pouliot J, Taschereau R, and Hsu I-C. Sensorless planning for medical needle insertion procedures. IEEE/RSJ International Conference on Intelligent Robots and Systems, 4:3337–3343, Oct. 2003.

[2]. Bicchi A and Kumar V. Robotic grasping and contact: a review. IEEE/RSJ International Conference on Intelligent Robots and Systems, 1:348–353, 2000.

[3]. Cai W, Hu SJ, and Yuan JX. Deformable sheet metal fixturing : Principles, algorithms, and simulations. Journal of Manufacturing Science and Engineering, 118(3):318–324, 1996.

[4]. Cavusoglu M, Tendick F, Cohn M, and Sastry S. A laparoscopic telesurgical workstation. IEEE Transactions on Robotics and Automation, 15(4):728–739, 8 1999.

[5]. Cheong J-S, Goldberg K, Overmars M, and van der Stappen A. Fixturing hinged polygons. IEEE International Conference on Robotics and Automation, 1:876–881, 2002.

[6]. Fichtinger G, Burdette EC, Tanacs A, Patriciu A, Mazilu D, Whitcomb LL, and Stoianovici D. Robotically assisted prostate brachytherapy with transrectal ultrasound guidance–phantom experiments. Brachytherapy, 5(1):14–26, Jan. 2006. [PubMed: 16563993]

[7]. Gopalakrishnan KG and Goldberg K. D-space and deform closure grasps of deformable parts. The International Journal of Robotics Research, 24(11):899–910, 2005.

[8]. Guthart G and Salisbury J, J.K. The intuitive™telesurgery system: overview and application. IEEE International Conference on Robotics and Automation, 1:618–621 vol.1, 2000.

[9]. Hirai S, Tsuboi T, and Wada T. Robust grasping manipulation of deformable objects. In IEEE International Symposium Assembly and Task Planning, 5 2001.

[10]. Holleman C, Kavraki L, and Warren J. Planning paths for a flexible surface patch. IEEE International Conference on Robotics and Automation, 1:21–26, 5 1998.

[11]. Howard AM and Bekey GA. Recursive learning for deformable object manipulation. In Proceedings of the 8th International Conference on Advanced Robotics, pages 939–944, 1997.

[12]. Irving G, Teran J, and Fedkiw R. Invertible finite elements for robust simulation of large deformation. Symposium on Computer Animation, pages 131–140, 2004.

[13]. Lamiraux F and Kavraki LE. Path planning for elastic plates under manipulation constraints. In IEEE International Conference on Robotics and Automation, pages 151–156, 1999.

[14]. Madhani A, Niemeyer G, and Salisbury J, J.K. The black falcon: a teleoperated surgical instrument for minimally invasive surgery. IEEE/RSJ International Conference on Intelligent Robots and Systems, 2:936–944, 10 1998.

[15]. Mallapragada V, Sarkar N, and Podder T. Robot assisted real-time tumor manipulation for breast biopsy. In IEEE International Conference on Robotics and Automation, 2008.

[16]. Menassa R and Vries WD. Optimization methods applied to selecting support positions in fixture design. ASME Journal of Engineering for Industry, 113:412–418, 1991.

[17]. Moll M and Kavraki L. Path planning for deformable linear objects. IEEE Transactions on Robotics, 22(4):625–636, Aug. 2006.

[18]. Rodriguez S, Lien J-M, and Amato NM. Planning motion in completely deformable environments. In IEEE International Conference on Robotics and Automation, pages 2466–2471, Orlando, FL, 5 2006.

[19]. Saha M and Isto P. Motion planning for robotic manipulation of deformable linear objects. IEEE International Conference on Robotics and Automation, pages 2478–2484, 5 2006.

[20]. Sutherland G, McBeth P, and Louw D. Neuroarm: An mr compatible robot for microsurgery. In Computer Assisted Radiology and Surgery, volume 1256, pages 504–508, 2003.

[21]. Taylor R, Jensen P, Whitcomb L, Barnes A, Kumar R, Stoianovici D, Gupta P, Wang Z, Dejuan E, and Kavoussi L. A Steady-Hand Robotic System for Microsurgical Augmentation. The International Journal of Robotics Research, 18(12):1201–1210, 1999.

[22]. Taylor RH. Robots as surgical assistants: Wher we are, wither we are tending, and how to get there. In AIME ‘97: Proceedings of the 6th Conference on Artificial Intelligence in Medicine in Europe, pages 3–11, London, UK, 1997 Springer-Verlag.

[23]. Tombropoulos RZ, Adler JR, and Latombe J. Carabeamer: A treatment planner for a robotic radiosurgical system with general kinematics. Medical Image Analysis, 3:3–3, 1999.

[24]. Torabi M, Hauser K, Alterovitz R, Duindam V, and Goldberg K. Guiding needle insertions using single-point tissue manipulation. In IEEE International Conference on Robotics and Automation, 5 2009.

[25]. Yu X, Chizeck HJ, and Hannaford B. Comparison of transient performance in the control of soft tissue grasping. In IEEE/RSJ International Conference on Intelligent Robots and Systems, San Diego, CA, 10 2007.

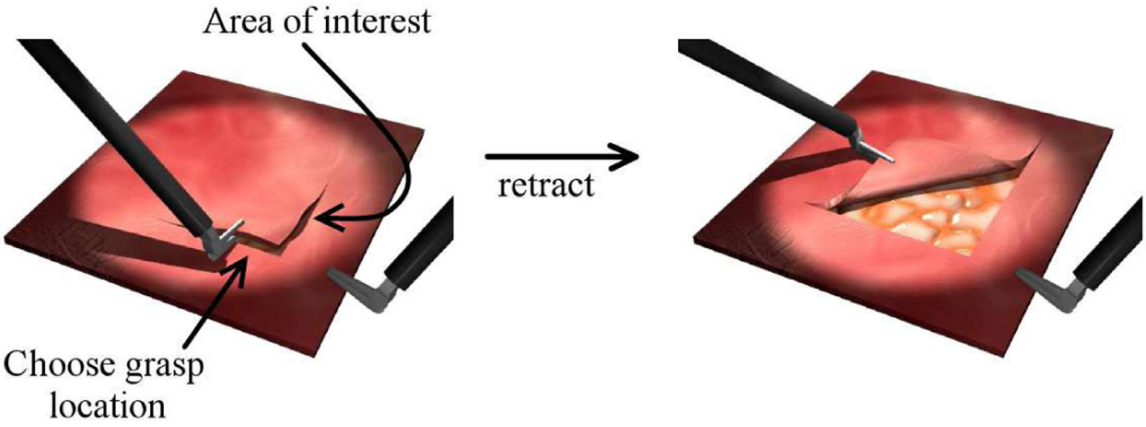

Fig. 1:

The process of retracting a layer of tissue. The surgeon identifies an area of interest and makes incisions in order to retract the overlying tissue. Tool tips should be optimally placed to minimize maximum strain.

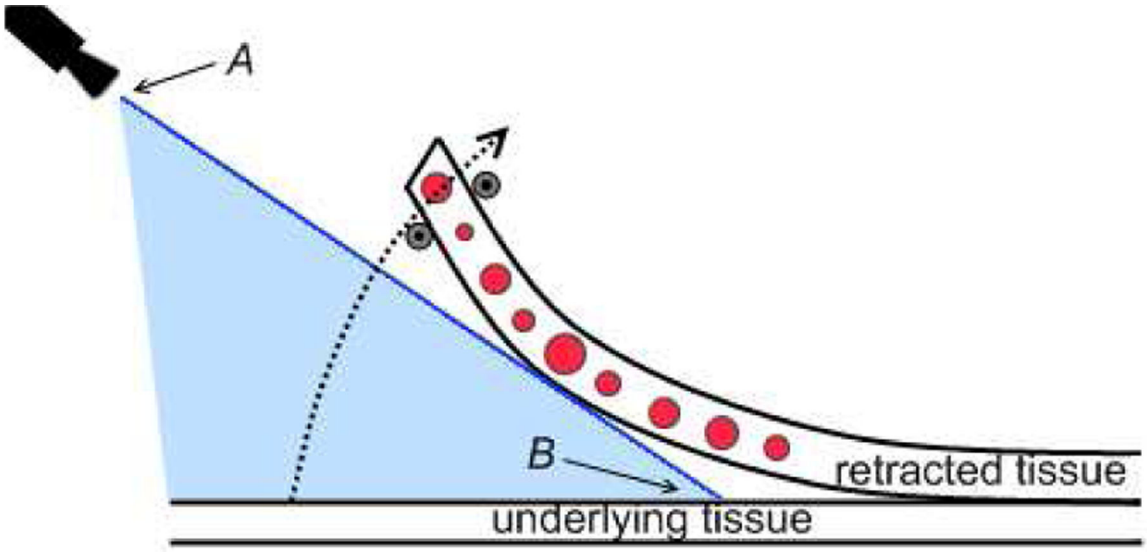

Fig. 2:

2D tissue retraction problem. The tissue is considered heterogeneous and we are concerned with visibility and accessibility of the area of interest. *A* denotes the position of a camera and *B* the most distant location on the area of interest. The RSA should move the tissue to lie completely outside the shaded region, above *AB*, enabling visibility to the camera.

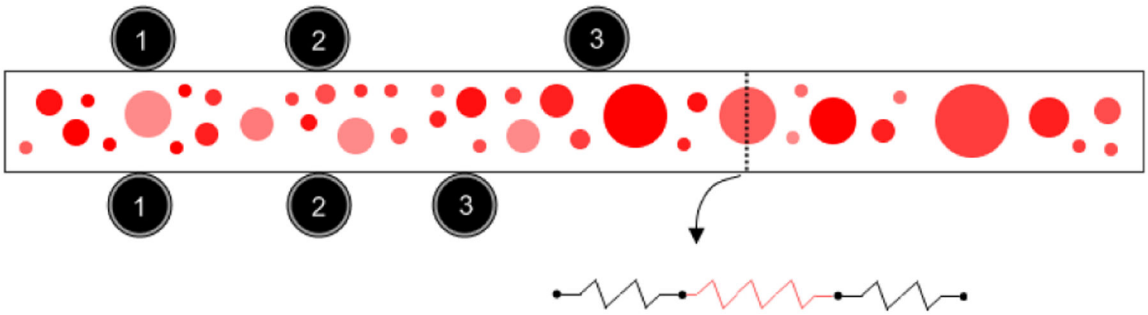

Fig. 3:

A continous model for representing heterogeneous tissue. Darker shaded areas represent veins. Jaws as shown in positions 1 and 2 (but not 3) are allowed, as they are opposite from each other on the tissue. When considering a line segment running from the upper surface to the lower surface between the jaws, we regard it as a serial connected spring with varying spring constants.

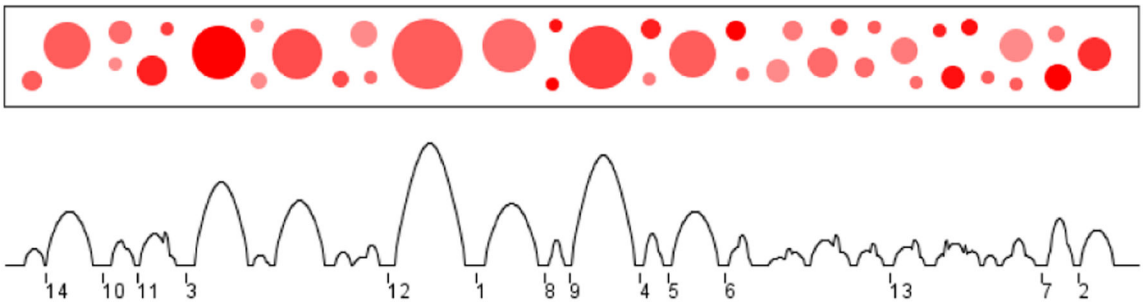

Fig. 4:

Above: The 2D model representing the heterogeneous tissue. Below: A plot of the equivalent spring constant function along the tissue and quality ranking for stable grasps.

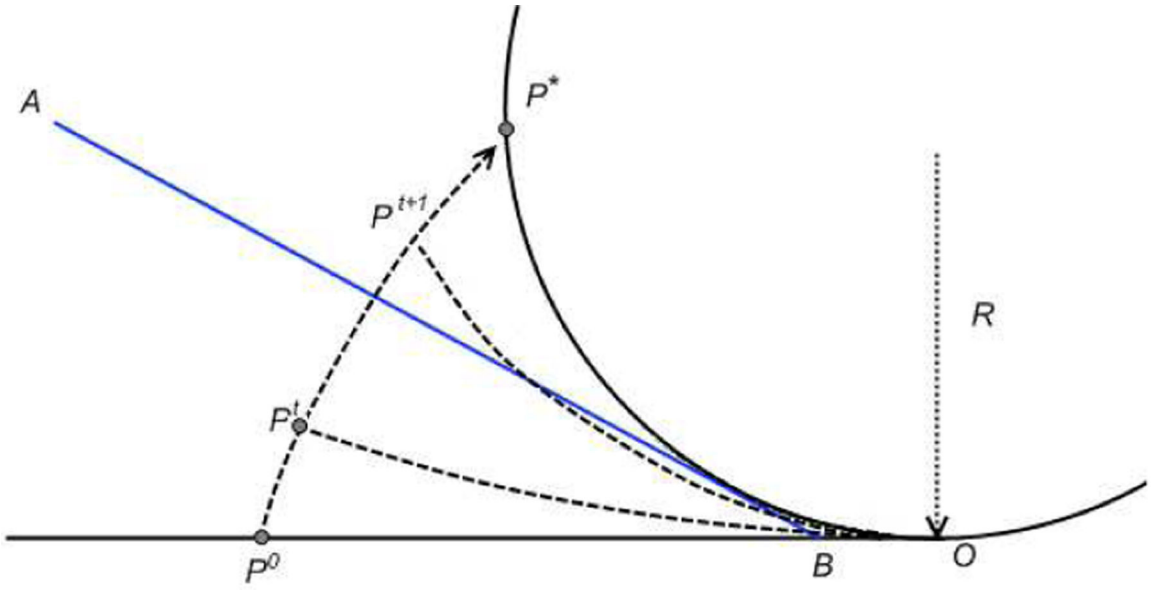

Fig. 5:

An optimal final configuration p_g for the medial axis point p_0 at distance x from the fixed end will lie on the circle having radius R, intersects the origin O and is tangent to the line-of-sight AB. Keeping each intermediate configuration optimal, p_0 must remain on the end of a circular arc with curve length x, and intersecting the origin.

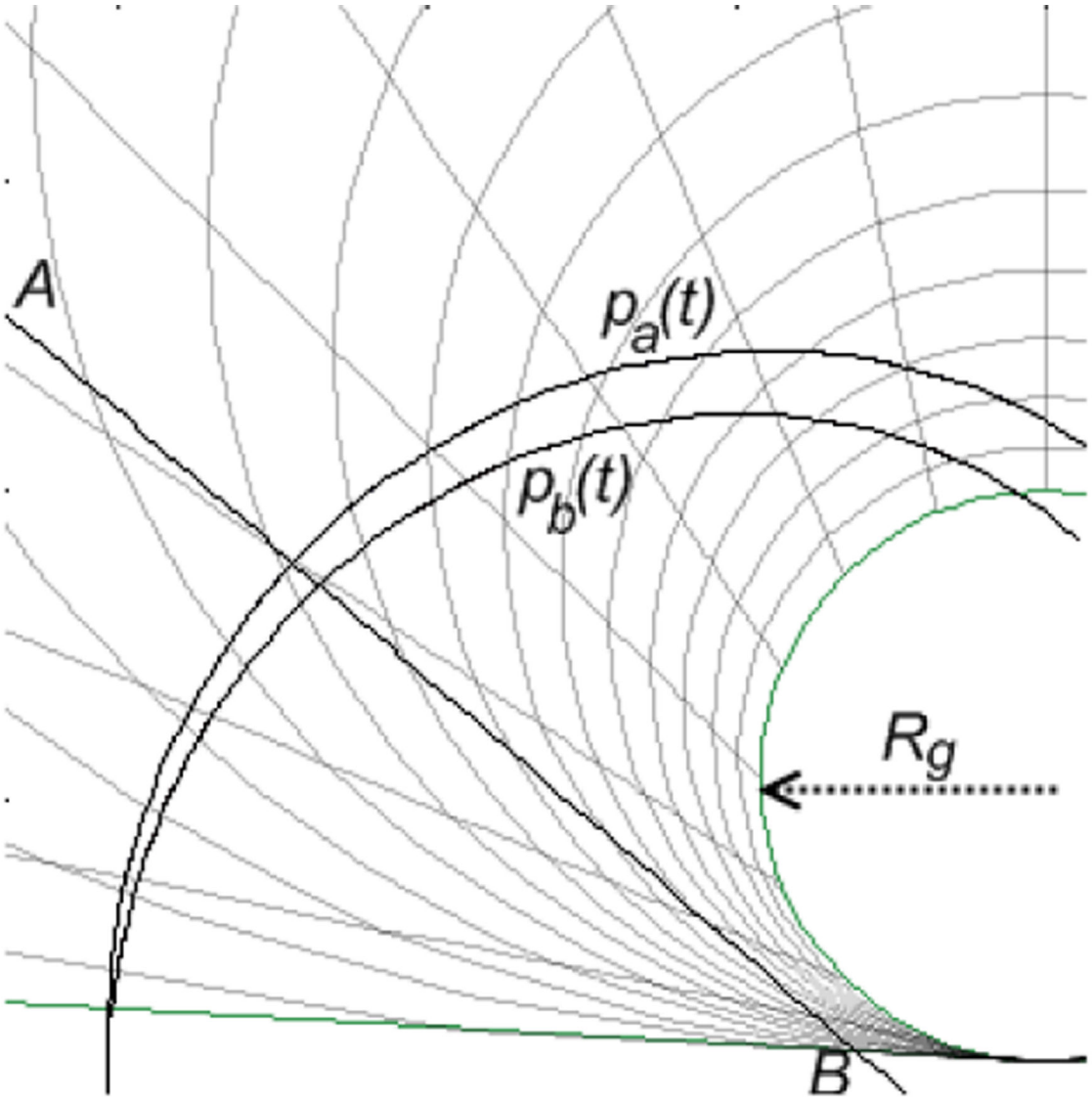

Fig. 6:
The trajectories $p_a(t)$ and $p_b(t)$ the jaw nodes follow during the retraction.

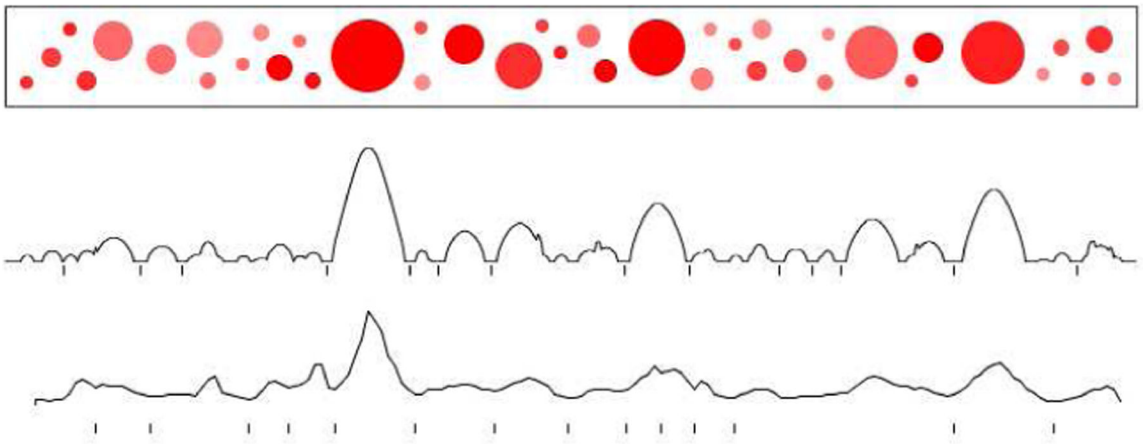

Fig. 7:

The tissue model and graphs showing stable grasp locations. The upper graphs was obtained by the spring method. The lower graph shows the results obtained from running brute-force simulations on all opposite perimeter nodes.

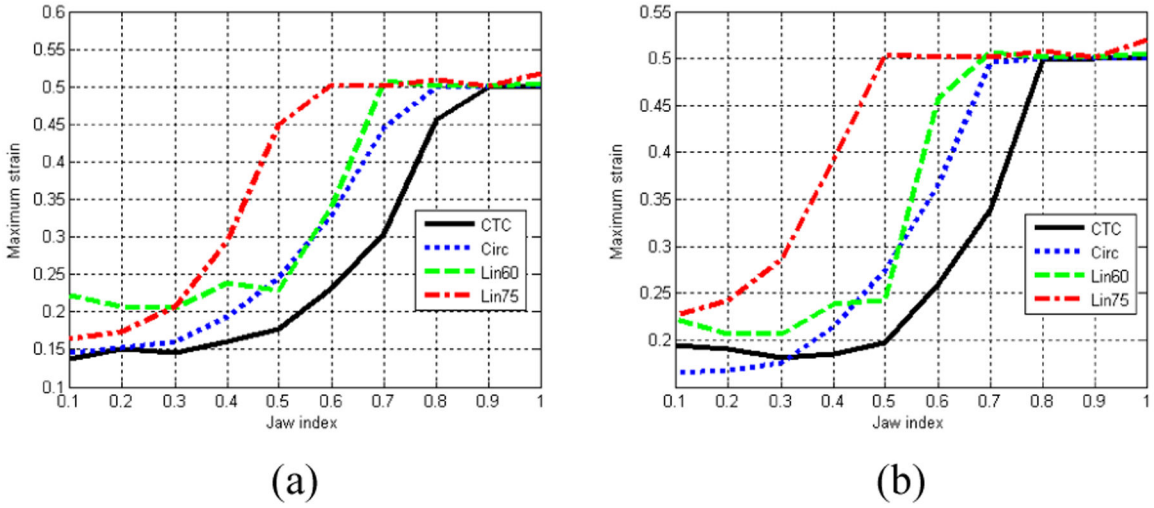

Fig. 8:

Comparison between linear, circular and the CTC trajectories for two lines-of-sight, starting at distance (a) 00025% and (b) 15% from the fixed end of the tissue. Each line-of-sight has 45° slope. Strain of 0.5 means failure. The CTC trajectories usually outperform the other trajectories, but circular trajectories perform slightly better for some grasp locations when the line-of-sight approaches the fixed end of the tissue.

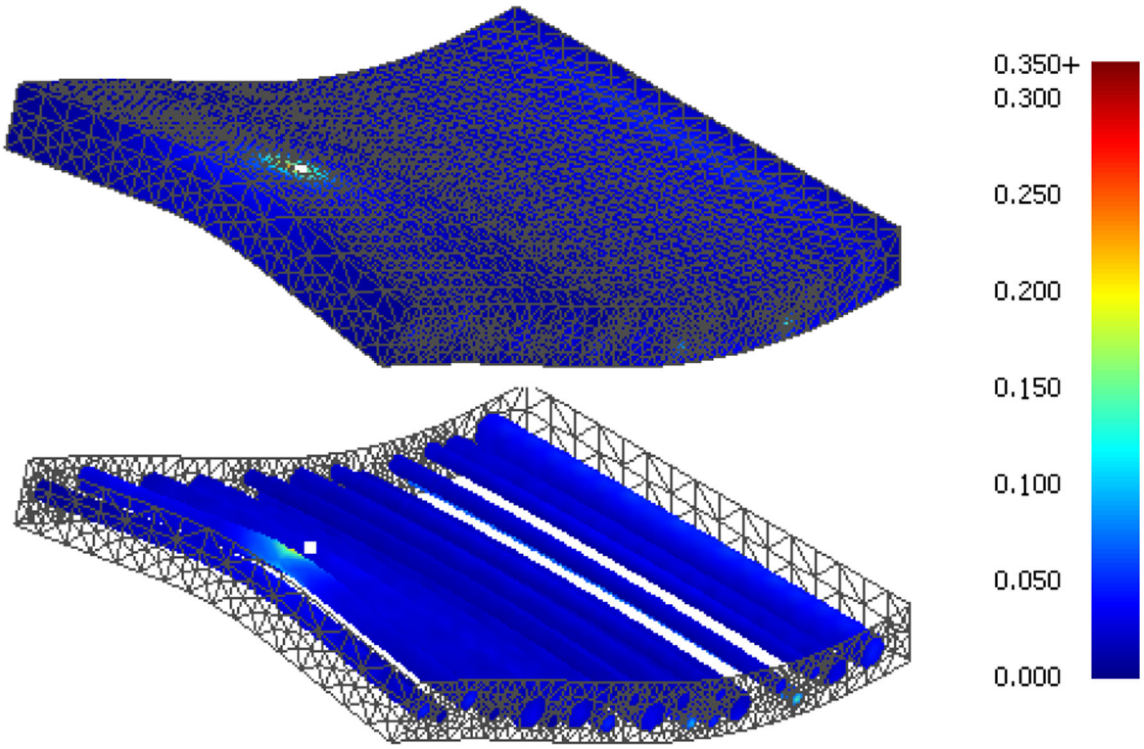

Fig. 9:

A screenshot of our 3D simulation on a heterogeneous mesh with 20 veins. The maximum strain is color coded. The top image shows the triangles on the surface of the mesh. Bottom image shows the strain on the veins. The depth is expanded to 3.5*cm*.

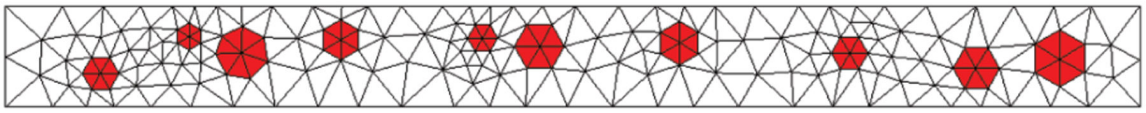

Fig. 10:
Side view of 3D FEM mesh containing 10 veins.

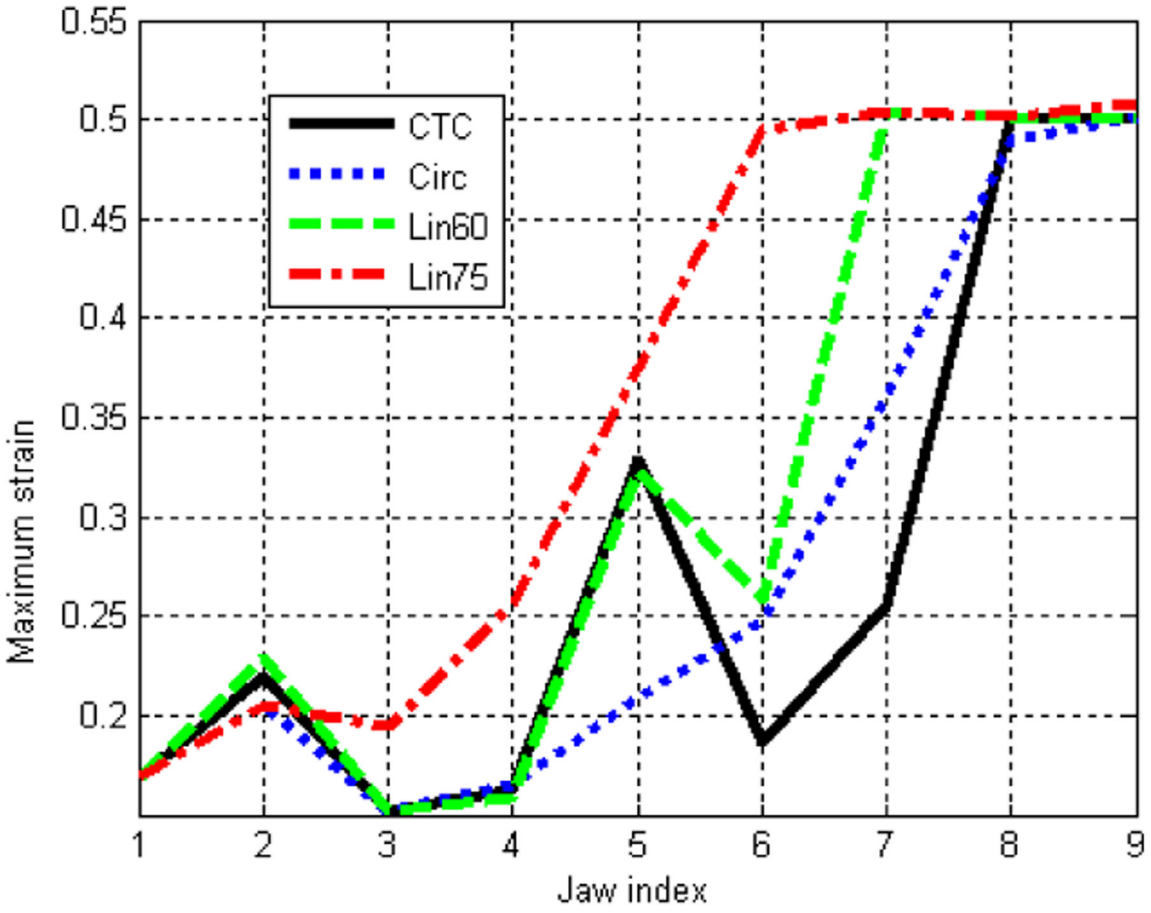

Fig. 11:

Comparison between various linear, circular, and constant-tissue-curvature (CTC) paths for heterogeneous tissue containing 10 veins. A jaw index of i means we contract at a stable location between the i-th and $(i + 1)$-th vein. The CTC path slightly outperforms the other paths.

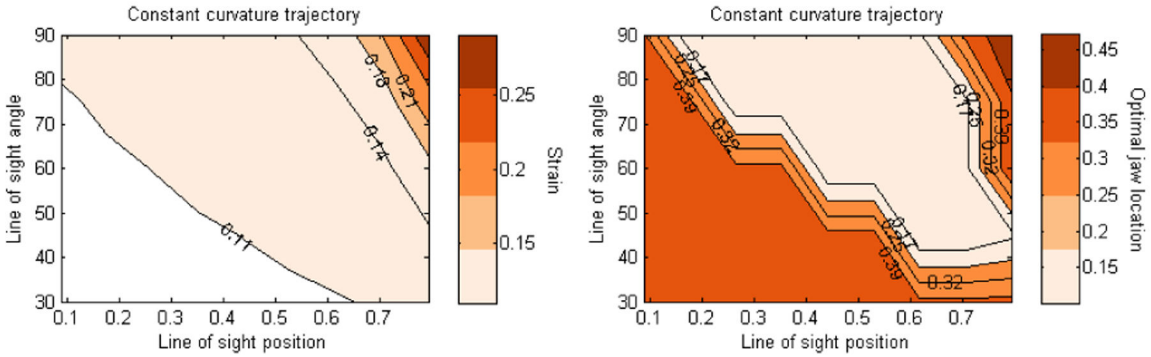

Fig. 12:

Showing optimal jaw locations and the resulting strains of our algorithm for various lines-of-sight in homogeneous tissue with strain limit of 0.5. The jaw location and the line-of-sight position are specified as the fraction of length from the open end of the tissue.